



HAL
open science

Stable milling of thin-walled parts with variable dynamics

Francisco Javier Campa, Sébastien Seguy, Luis Norberto López de Lacalle,
Lionel Arnaud, Gilles Desein, Gorka Aramendi

► **To cite this version:**

Francisco Javier Campa, Sébastien Seguy, Luis Norberto López de Lacalle, Lionel Arnaud, Gilles Desein, et al.. Stable milling of thin-walled parts with variable dynamics. Sixth International Conference High Speed Machining, Mar 2007, Saint-Sébastien, Spain. hal-03273545

HAL Id: hal-03273545

<https://hal.science/hal-03273545>

Submitted on 1 Jul 2021

HAL is a multi-disciplinary open access archive for the deposit and dissemination of scientific research documents, whether they are published or not. The documents may come from teaching and research institutions in France or abroad, or from public or private research centers.

L'archive ouverte pluridisciplinaire **HAL**, est destinée au dépôt et à la diffusion de documents scientifiques de niveau recherche, publiés ou non, émanant des établissements d'enseignement et de recherche français ou étrangers, des laboratoires publics ou privés.

Stable Milling of Thin-Walled Parts with Variable Dynamics

F.J. Campa¹, S. Seguy², L.N. López de Lacalle¹, L. Arnaud², G. Dessein², G. Aramendi³

¹University of the Basque Country, Bilbao, Basque Country, Spain

²École Nationale d'Ingénieurs, Tarbes, France

³Fundación Fatronik, San Sebastián, Basque Country, Spain

fran.campa@ehu.es sebastien.seguy@enit.fr

Abstract

The milling of thin-walled parts can become a seriously complex problem. In this work, the problem of the variable dynamics of a test part has been solved through the calculation of 3D stability lobes which add a third dimension with the tool position along the part, to the traditional depth of cut-spindle speed pair. First, the dynamics of a test part in several machining steps have been calculated through FEM analysis and validated through experimental tests. Then, the stable conditions have been calculated with a one-dimensional and a three-dimensional stability model for the thin walls and the thin floor respectively. Finally, several milling tests have been performed in order to validate the predictions made by the model.

Keywords

Chatter, Milling, Finite element method (FEM)

1 INTRODUCTION

These days, monolithic components are commonly used as structural parts in the aeronautical industry due to their homogeneity and excellent strength to weight ratio. Ribs, stringers, spars and bulkheads can be mentioned as an example. Monolithic parts are made of thin walls and webs, which confer enough stiffness to the whole part. Although they were usually made assembling several smaller parts, nowadays they are milled starting from a raw block of material and removing up to 95% of the weight of the initial block. Hence, a high productivity can only be achieved increasing the removal rate as much as possible. The drawback is that, at high removal rate conditions, the lack of stiffness of the thin walls and webs makes static and dynamic problems appear, particularly, the self-excited vibration called chatter, which is the most complex and difficult to avoid by manufacturers. As a consequence, unacceptable surface roughness levels, part damage and a lack of dimensional accuracy can be suffered.

However, the vibrations of the couple tool-part are known since the 1950's [1]. The first studies of the chatter machine-tool related to the continuous cutting processes, like the turning process, modelled with linear equations. Tlustý [2] succeeded in explaining the causes of these regenerative vibrations in the orthogonal case of the cut applied to turning. This knowledge is at the base of the stability lobes theory, which makes it possible to find the depth of cut according to the spindle speed, from which, the machining system will become unstable.

Studies on milling stability started later due to the complexity of modelling cutting forces, based on their variability in time and space. It is then about the middle of the 1990's, that the first modelling in analytical form appear [3], [4] and [5]. This theory is well applied in the case of the tools vibrations, because the dynamic characteristics are constant during all machining.

Methods dedicated to the highly interrupted cutting have only recently been developed. Davies [6] developed a frequency domain model by making the assumption that the time of cut is very small compared to the tooth period; this modelling is well adapted when the cut is strongly discontinuous. Davies [6], Gradisek [7], Bayly [8] showed that this conditions generated new stable zones inside unstable zones, due to period-doubling vibrations.

Chatter due to the excitation of the part has been also studied. In this case, this modelling cannot be applied directly, because the characteristics of the part strongly vary during machining [9], [10]. Budak [11] studied not only the static deflexion of the thin wall but also developed a frequency domain simulation for varying dynamics of the wall and tool in axial direction. The stability lobes change during machining what leads to the addition of the third dimension, corresponding to the tool position [12]. New improvements were made by the taking into account of the vibrations related to the machine and with the tool, let us quote in particular Bravo [13].

The case of thin floors has been less studied, maybe because it is a problem that traditionally has been solved with rigid fixtures. Smith [14] proposed the selection of tool with zero corner radius in thin floor machining since the regenerative vibration does not excite modes of the floor. 3D models were developed to take into account the movement of the floor, in particular Altintas [15] and Campa [16].

Our objective is to apply on the same part the modelling usually implemented for the machining of thin walls and thin floors. The following sections present the study. The section 2 present the part studied. The modelling based on finite element method calculus is shown in section 3. Section 4 present the stability model based on frequency analysis. The section 5 exposes the experimental work, the tests carried out, the surface roughness analysis, and the correlation with the modelling. Sections 6 conclude this work and present the prospects.

2 STUDIED PART

In order to have a part representative of the aeronautical milling problems, the study was focused on a part with the typical shape of a "pocket", see Figure 1.

This part is made of two distinct types of thin walls: the floor and the lateral wall. The workpiece is made in an aluminium alloy 7075T6 like structural parts. The dimensions are chosen in order to correlate with an industrial part. The thicknesses of the walls after machining are respectively of 1mm for the floor and 3 mm for the walls.

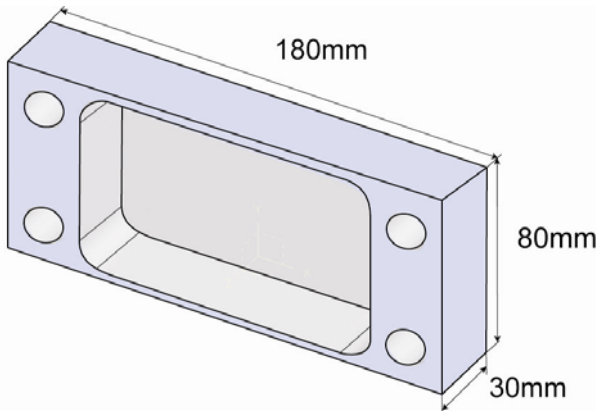


Figure 1: Workpiece size.

The dynamic characteristics of this part are very complex, it can't be represented by a simple mass spring. This part is characterized by several modes with specific modal shapes, so their corresponding natural frequencies, stiffnesses and damping ratios must be calculated.

For industrial partners, the evaluation of the manufacture of the structures is based on standard criteria. In the case of structural parts for aeronautical purposes, the following criteria are typical:

- Surface roughness: 3.2 μm .
- Dimension tolerance: ± 0.15 mm.
- Geometrical flatness: 0.15mm in the whole area and 0.05 mm in a straight direction.

3 FEM CALCULATION

The pocket machining has been divided in two operations. First, the pocketing of the floor has been carried out with a bull nose end mill, and then the finishing of the wall has been made with an end mill.

Due to the variety of parameters involved, there are endless possibilities to do the pocketing, such as: the axial and radial depth of cut, down-milling or up-milling, strategy, initial thickness of the floor, etc. To simplify, it was decided to fix the strategy, the radial immersion $A_e = 10\text{mm}$, and the type of cut, down-milling. The initial thickness of the floor and consequently the axial depth of cut A_p are chosen through iteration calculating the modal parameters and the corresponding stability lobes. If the initial thickness is too small the lobes indicate that the milling is almost impossible to do, and if it is too thick the possibility of chatter appearance vanishes, so a compromise was taken. The spindle speed N was chosen according to the stable areas in the lobes diagram. After several tests, a parallel strategy type "outgoing" for the machining of the floor was selected, see Figure 3, whereas the machining of the side wall was carried out in contouring.

During the machining, the part dynamic characteristics evolve according to the tool position and the removal of material. The natural frequency decreases, during the machining. In order to predict this evolution, a traditional modelling by finite elements was used. The tool path was discretized; every 15 mm a modal analysis calculates the apparent stiffness and the natural frequency of the part. The part is modelled by plate elements, this assumption can easily be made in the case of thin wall, and reduce enormously the compute time. The model is parameterized in order to automate calculations.

As the precision of the calculated frequencies has to be better than 1%, hammer impact tests were conducted in order to adjust the finite element model to the real

behaviour of the part. These tests were made before the machining. The damping ratio was obtained by hammer test because it is impossible to predict accurately.

Figure 2 presents the second modal shape of the part. Note that all the walls (side and floor) are coupled. The machining of the floor involves the excitation of the side walls.

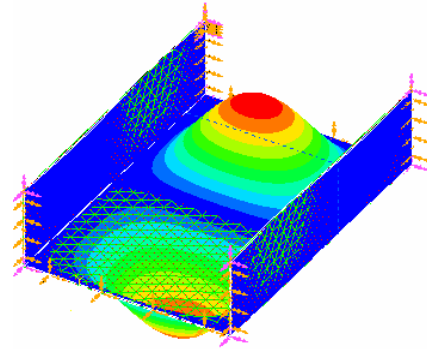


Figure 2: Modal shape of the second mode before machining.

Figure 3 shows the first 4 modes natural frequencies evolution in the case of the floor machining. For the tests, the axial depth of cut was finally fixed at $A_p = 5$ mm (6 to 1 mm thick). The strategy of milling modelled consisted on a ramp-down milling (step1), return, followed by four alternating cuts in down-milling (steps 2 to 5). During the machining of the floor, the natural frequencies change considerably. The first mode evolves from 3.25 kHz to 1.7 KHz.

For the machining of the thin wall, being a finish milling, the material removal is little, 0.1 mm of axial depth of cut. In this case, only the apparent stiffness varies according to the tool position [12]. The stability lobes are only computed on the centre of the wall, where the stiffness is lower.

4 STABILITY ANALYSIS MODEL

From the modal characteristics obtained by calculations and validated by tests, we can study the machining stability. For that, we quickly will present the models used for the floor and the side wall. The model here presented is based on the Budak and Altintas work [3], [4], [15] and the averaging proposed in [16].

4.1 Floor

Dynamic Chip Thickness Calculation

The cutting edge j cuts a dynamic chip thickness h_j that is calculated as a function of the difference of position between the actual edge and the previous edge that passed in that point, as in [16]:

$$h_j = [\Delta x \cdot \sin(\phi_j) + \Delta y \cdot \cos(\phi_j)] \cdot \sin(\gamma) + \Delta z \cdot \cos(\gamma) \quad (1)$$

Calculation of the Cutting Forces

The forces model relates the cutting forces with the dynamic displacements through (2). The characterization of the specific cutting coefficients is based on a mechanistic model. Hence, the cutting forces, tangential f_t , radial f_r and axial f_a , are:

$$\begin{Bmatrix} f_t \\ f_r \\ f_a \end{Bmatrix} = K_t \cdot a \cdot \begin{Bmatrix} 1 \\ K'_r \\ K'_a \end{Bmatrix} \cdot h_j(\phi_j) \quad (2)$$

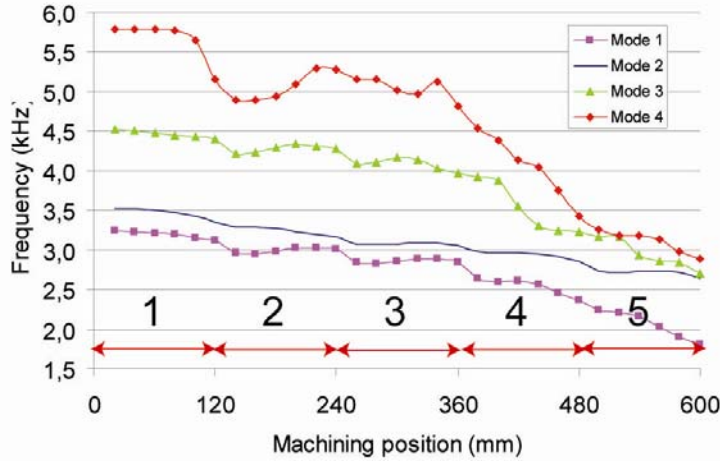


Figure 3: Natural frequency evolution for the floor machining.

where K_r' and K_a' are the specific radial and axial shearing coefficients 'normalized' to K_t . Those forces are projected over the Cartesian axes as follows:

$$\begin{cases} f_x \\ f_y \\ f_z \end{cases} = \begin{bmatrix} -\cos \phi_j & -\sin \gamma \cdot \sin \phi_j & \cos \gamma \cdot \sin \phi_j \\ \sin \phi_j & -\sin \gamma \cdot \cos \phi_j & \cos \gamma \cdot \cos \phi_j \\ 0 & -\cos \gamma & -\sin \gamma \end{bmatrix} \begin{cases} f_t \\ f_r \\ f_a \end{cases} \quad (3)$$

Substituting (2) in (3) and summing the forces for all the cutting edges N , forces and displacements get related by the matrix of directional coefficients $[\mathbf{A}(t)]$ in (4).

$$\{\mathbf{f}(t)\} = \frac{1}{2} \cdot A_p \cdot K_t \cdot [\mathbf{A}(t)] \cdot \{\Delta(t)\} \quad (4)$$

Calculation of the Stability Limit

The incremental displacement for a given period of cut T is:

$$\{\Delta(t)\} = (1 - e^{-i\omega_c T}) \cdot [\mathbf{G}(i\omega_c)] \cdot \{\mathbf{f}\} e^{i\omega_c t} \quad (5)$$

Where $[\mathbf{G}(i\omega_c)]$ includes the frequency response functions of both the tool and workpiece. Introducing (5) in (4), the following equation is obtained:

$$\{\mathbf{f}(t)\} = \frac{1}{2} \cdot A_p \cdot K_t \cdot (1 - e^{-i\omega_c t}) \cdot [\mathbf{A}(t)] \cdot [\mathbf{G}(i\omega_c)] \cdot \{\mathbf{f}(t)\} \quad (6)$$

An analytical solution for (6) can be found, substituting the periodic matrix $[\mathbf{A}(t)]$ by its average term in the Fourier series expansion. Hence, (6) becomes an eigenvalue problem, where (7) defines the stability, and the eigenvalue is (8):

$$\det[[\mathbf{I}] + \lambda \cdot [\mathbf{G}_0(i\omega_c)]] = 0 \quad (7)$$

$$\lambda = -\frac{z}{2\pi} \cdot A_p \cdot K_t \cdot (1 - e^{-i\omega_c T}) \quad (8)$$

As in [2], the critical depth of cut $A_{p\text{lim}}$ and the corresponding spindle speeds N for each lobe m are obtained as:

$$A_{p\text{lim}} = -\frac{2\pi}{z \cdot K_t} \cdot \text{Re}(\lambda) \cdot \left[1 + \left(\frac{\text{Im}(\lambda)}{\text{Re}(\lambda)} \right)^2 \right] \quad (9)$$

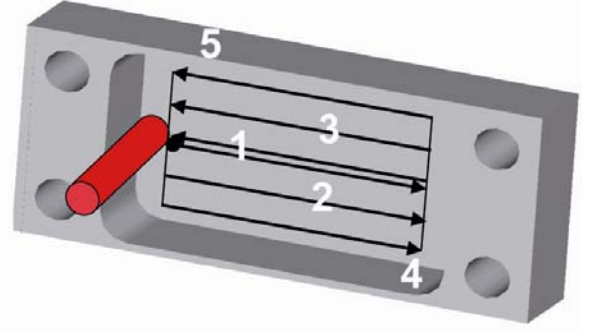


Figure 4: Floor modelling.

Averaging

For bull-nose end mills with a corner radius r_0 , the angle κ is variable along the tool axis direction, so it is necessary to find an average value to solve the stability problem. The same has to be done with the cutting coefficients as they vary due to the helix angle. The method here presented averages the cutting edge lead angle at the middle of the cutting arc, κ_{m1} , over the volume of the chip for a given depth of cut A_p , so average values can be obtained. When A_p is lower than the corner radius:

$$\kappa_{m1} = \arccos((r_0 - z) / r) \quad (12)$$

$$r_{m1} = (R - r_0) + r_0 \cdot \sin \kappa_{m1} \quad (13)$$

$$\text{Thus, } \bar{\kappa} = \frac{\int_0^{A_p} \int_{\phi_0}^{\phi_1} \left(\frac{\kappa_{m1}}{2} f_z \sin(\phi) r_{m1} m \right) d\phi dz}{\int_0^{A_p} \int_{\phi_0}^{\phi_1} (f_z \sin(\phi) r_{m1} m) d\phi dz} \quad (14)$$

$$\text{Where: } m = \frac{d\kappa}{dz} = 1 / \left(r_0 \sqrt{1 - \frac{(r_0 - z)^2}{r_0^2}} \right) \quad (15)$$

On the other hand, when the depth of cut is higher than the corner radius:

$$\kappa_{m2} = \frac{(r_0 \cdot \pi / 2 \cdot \pi / 4 + (z - r_0) \pi / 2)}{(r_0 \cdot \pi / 2 + (z - r_0))} \quad (16)$$

$$\bar{\kappa} = \frac{\int_0^{r_0} \int_0^{\phi_0} \left(\frac{\kappa_{m1}}{2} f_z \sin(\phi) r_{m1} m \right) d\phi dz + \int_0^{r_0} \int_0^{\phi_0} \left(R \frac{\kappa_{m2}}{2} f_z \sin(\phi) \right) d\phi dz}{\int_0^{r_0} \int_0^{\phi_0} (f_z \sin(\phi) r_{m1} m) d\phi dz + \int_0^{r_0} \int_0^{\phi_0} (R f_z \sin(\phi)) d\phi dz} \quad (17)$$

Therefore the average axial immersion angle is $\bar{\gamma} = 180^\circ - \bar{\kappa}$ and the average height $\bar{z} = r_0 - r_0 \cdot \cos(\bar{\kappa})$.

4.2 Wall

Initial Assumptions

The tool is rigid compared to the workpiece, which is considered to be flexible.

The workpiece moves only on the y direction, like a single degree of freedom, see Figure 5.

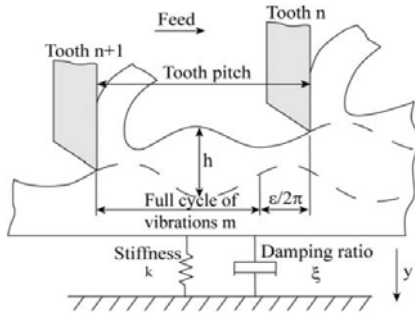


Figure 5: Wall modelling.

The transfer function of the part in the direction is there:

$$G_y(i\omega_c) = \frac{\omega_0^2}{k(\omega_0^2 - \omega_c^2 + 2\xi\omega_0\omega_c i)} \quad (18)$$

We use a linear cutting law where: $f_T = K_T A_P A_E$ and $f_R = K_R F_T$ where K_T and K_R are the tangential and radial cutting force.

Result

Our goal is only to use the model, we directly will give the equations allowing the calculation of the stability lobes [4]. The axial depth of cut limit is expressed in the

$$\text{form: } A_{P\text{lim}} = \frac{1}{\frac{z}{2\pi} \alpha_{yy} K_T \text{Re}[G_y(i\omega_c)]} \quad (19)$$

Where z is the teeth number, and α_{yy} the directional milling coefficient:

$$\alpha_{yy} = \frac{1}{2} [-\cos(2\theta) - 2K_R\theta - K_R \sin(2\theta)]_{\phi_{ST}}^{\phi_{EX}} \quad (20)$$

Where θ is the tool angle engagement, ϕ_{EX} and ϕ_{ST} the exit and start angles. $\text{Re}[G_y(i\omega_c)]$ is the real part of the structural transfer function of a system with one degree of freedom:

$$\Re[G_y(i\omega_c)] = \frac{1}{k} \frac{1 - d^2}{(1 - d^2)^2 - 4\xi^2 d^2} \quad (21)$$

Where $d = \frac{\omega_c}{\omega_0}$, ω_0 the natural pulsation, k the stiffness

and ξ the damping ratio. The link between the chatter frequency ω_c and the spindle speed, is:

$$N = \frac{60\omega_c}{z \left[2m\pi + 2\pi - 2\arctan \left[\frac{d^2 - 1}{2\xi d} \right] \right]} \quad (22)$$

The equations (19) and (22) constitute a system of equations parameterized in m and ω_c , it is then possible to plot the stability lobes of for each mode of vibration of the wall.

5 EXPERIMENTAL WORK

The cutting tests were carried out on a 3-axis high speed milling machine, with a 24000 rpm spindle. The tool for the thin wall was an end mill with four flutes, a diameter of 12 mm, 45° helix angle and a corner radius of 0.15 mm. The cutting coefficients are $K_t = 700\text{MPa}$, and $K_r = 0.3$. For the floor a bull-nose end mill was selected with a diameter of 16mm, 2 teeth, and a corner radius of 2.5 mm, 30° helix angle. The cutting coefficients for the bullnose part are $K_t = 1723,3-369,44 \cdot z$, $K_r = 558,35-198,93 \cdot z$, $K_a = 48,26+52,15 \cdot z$, and for the frontal part $K_t = 804,73$, $K_r = 65,495$ and $K_a = 174,02$. The fixture leaves free the wall side and the floor, see Figure 6.

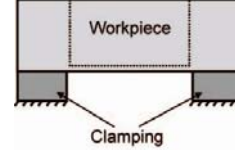


Figure 6: Machining set-up.

5.1 Experimental test

Floor

The floor was machined in five steps as it is explained in Section 3 with a feedrate of 0.05 mm/tooth. Two tests were carried out. Test A, at the maximum spindle speed, 24000 rpm, and test B, selecting, for each step, an optimal spindle speed using the stability lobes. The lobes calculated didn't allow machining the whole part with a single spindle speed. So, for test B, the spindle speed was 24000, 21550, 21300, 19650 and 20000 rpm for steps 1, 2, 3, 4 and 5 respectively, see Figure 7.

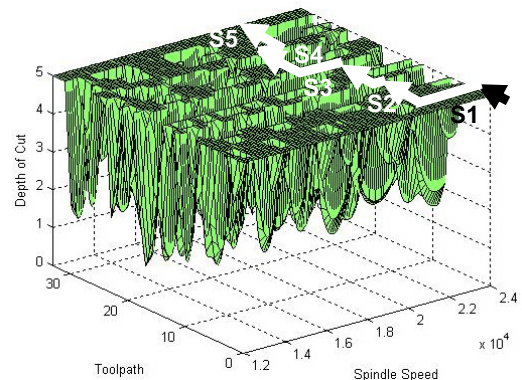


Figure 7: 3D Stability lobes for the floor testing.

Wall

The wall was down-milled in finishing with axial depth of cut of 5 and 3 mm, a radial immersion of 0.1 mm, and a feedrate of 0.05 mm/tooth, with the second tool. The spindle speed is chosen with the stability lobes [12], see Figure 8. In this case, it is the maximum: 24000 rpm.

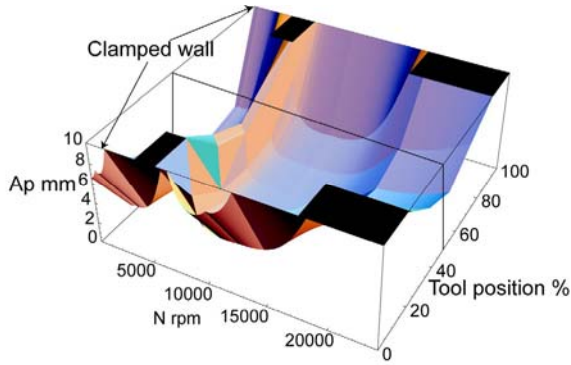


Figure 8: 3D Stability lobes for the wall.

5.2 Results

Floor

The study of the floors has been approached focusing on each area of each of the five steps, instead of considering every step as a whole. The measurements are summarized in Table 1 and Table 2, surface location error and surface roughness in R_a , where cells with grey background mean out of the tolerances in Section 2.

	s4	s2	s1	s3	s5
1	4,67	4,75	10,50	0,33	-4,83
2	-9,00	2,25	2,00	-3,60	-12,00
3	-21,60	-3,29	-9,20	-17,40	-19,83
4	-18,33	-0,50	2,50	-16,43	-24,40
5	-10,71	11,60	15,80	-15,11	-24,40
6	1,00	12,80	17,86	-14,40	-3,00
max step	26,27	16,09	27,06	17,73	21,40

	s4	s2	s1	s3	s5
1	4,83	0,50	14,83	-7,33	-8,50
2	-10,83	-9,40	23,67	-24,00	-15,00
3	-22,29	-9,50	31,43	-36,14	-26,00
4	-21,20	-4,38	25,14	-50,00	-26,83
5	-15,00	0,33	20,67	-27,86	-26,83
6	-1,33	0,29	20,20	-18,00	-8,75
max step	27,12	10,00	16,60	42,67	18,33

Table1: Surface location error in μm of each area of the part. Above) Test A. Below) Test B.

	s4	s2	s1	s3	s5
1	0,46	0,83	1,13	0,83	0,69
2	2,04	1,15	2,29	0,38	0,89
3	2,67	1,50	3,86	0,67	2,02
4	3,12	2,36	1,92	1,77	3,17
5	1,55	1,19	0,70	1,57	1,32
6	1,28	1,01	0,73	1,24	1,14

	s4	s2	s1	s3	s5
1	1,62	2,80	0,73	0,86	1,18
2	2,69	0,91	0,93	2,04	1,27
3	3,12	1,04	0,72	1,17	0,67
4	2,81	1,05	0,91	1,62	0,32
5	1,58	0,71	0,52	1,30	0,65
6	0,93	0,93	0,30	1,56	1,43

Table 2: Surface roughness R_a in μm of each area of the part. Above) Test A. Below) Test B.

	s4 (↓)		s2 (↓)		s3 (↑)		s5 (↑)	
	p	m	p	m	p	m	p	m
1	s	s	s	s	s	s	s	s
2	u/s	u	u	s	u	u	s	u
3	u	u	u	u	u	u	s	u
4	u	u	u	u	u	u	u	u
5	s	u	u	u	u	u	u	u
6	s	u	s	u	s	s	s	u

	s4 (↓)		s2 (↓)		s3 (↑)		s5 (↑)	
	p	m	p	m	p	m	p	m
1	s	s	s	s	s	u	s	s
2	u/s	s	s	s	s	u	s	u
3	u/s	u	u/s	s	u/s	u	s	s
4	u/s	u	u/s	u	u/s	u	s	s
5	s	u	s	s	u/s	s	s	s
6	s	s	s	s	s	s	s	s

Table 3: Predicted (p) and measured (m) stability for each area of the part. Above) Test A. Below) Test B.

The surface location error is measured as the relative height of each area in microns related to the surface created with the four corners of the part. Max step in the bottom is the maximum step in height along the vertical line.

Table 3 shows the predicted and measured stability in each floor, where 's' means stable, 'u' unstable and 'u/s' means that the cutting conditions selected are 0,5 mm above/below limit of stability. The measurement was made through the analysis of the Fourier spectrum of the noise during the machining.

Not always the predicted matches the measured, though. The reason can be found in the changing modal parameters and tool position, which result in a delay in the chatter appearance. This means that cases predicted as unstable are stable, e.g. rows 4-1 in step 3 of test B. Also, once chatter appears, when stable conditions are reached again, it takes some time to recover the stability. This results in cases with predicted stability that are unstable, e.g. rows 2-3 in step 2 of test A.

Wall

The tests on the side walls gave a stable machining for a depth of cut of 3mm, but on the other hand, machining was unstable for a depth of cut of 5mm (predicted by the lobes). The depth of real cut is lower than the depth of calculated cut. We then note the importance of the assumptions of modelling, Section 4.2. In fact we use a simple model, with many assumptions, for a complex part.

5.3 Comparison

Floor

Regarding the surface location error, in both tests the tool tends to overcut especially in the most flexible areas, rows 3 and 4 in Table 1. In general, the overcut is higher in the test B, and it could be explained by the higher forced vibration when machining near a modal frequency. On the other hand, it can't be said that stability always leads to a higher overcut.

Comparing the surface finish, there is very little difference between test A and test B, see Figure 9. Again it is very difficult to relate the surface finish to the stability of the milling. Not always the finish is better in the stable areas. There is only one case out of tolerances, in test A, but even narrowing the requirements in R_a , there would be both stable and unstable cases out of tolerances.



Figure 9: Left) Test B. Right) Test A.

Wall

The machining of the wall is less difficult, because it has less modes of vibration, and little material removal, see Figure 8. The 3D lobes make possible to understand better the phenomena: near the clamping, the depth of cut increases. There remain inaccuracies in the modelling, in particular in the cutting law coefficient in finishing [9].

6 CONCLUSIONS

The prediction of stability in real parts is a very complex problem. Depending on the geometry, different models have to be used, for thin walls and thin floors. The removal of material implies that the modal parameters are continuously changing, as well as the tool position over the part. In addition, depending on the part, at high speed cutting conditions several high frequency modes can be involved in the calculus.

The 3D stability lobes plot the traditional stability lobes along the toolpath, so the most productive stable conditions can be chosen. However, depending on the complexity of the part and the change in the modal parameters, several spindle speeds or at least a continuously changing spindle speed must be selected. This approach can be problematic in an industrial context because not all the spindles allow such variations, so it may only be effective with simpler geometries. A good example of the use of these techniques has been made in this paper.

In prospects, we are working on the improvement of the model to limit the assumptions. Also, it will be interesting to show other optimisation solutions like, the variable pitch tool, the spindle speed variation...

7 ACKNOWLEDGMENTS

The authors acknowledge the co-financial support of the European Union by means of the Interreg IIIa Action AEROSFIN (The Pyrenees Manufacturing Aeronautical Spanish-French Interregional Network).

8 REFERENCES

[1] Tobias, S.A., Fishwick, W., 1958, A theory of regenerative chatter, The Engineer, London.
 [2] Tlustý, J., Poláček, M., 1963, The stability of machine tool against self excited vibrations in machining,

International Research in Production Engineering, 465-474.

[3] Budak, E., Altintas, Y., 1998, Analytical prediction of the chatter stability in milling - Part I: General formulation, Journal of Dynamic Systems, Measurement and Control, 120:22-30.
 [4] Budak, E., Altintas, Y., 1998, Analytical prediction of the chatter stability in milling - Part II: Application of the general formulation to common milling systems, Journal of Dynamic Systems, Measurement and Control, 120:31-36.
 [5] Jensen, S.A., Shin, Y.C., 1999, Stability analysis in face milling operation, Part - I: Theory of stability lobe prediction, Journal of Manufacturing Science and Engineering, 121:600-605.
 [6] Davies, M.A., Balachandran, B., 2000, Impact dynamics in milling of thin walled structures, Nonlinear Dynamics, 22:375-392.
 [7] Gradisek, J., Kalveram, M., Insperger, T., Weinert, K., Stepan, G., Govekar, E., Grabec, I., 2005, On stability prediction for milling, International Journal of Machine Tool and Manufacture, 45:769-781.
 [8] Bayly, P.V., Halley, J.E., Mann, B.P., Davies, M.A., 2003, Stability of interrupted cutting by temporal finite element analysis, Journal of Manufacturing Science and Engineering, 125:220-225.
 [9] Lapoujoulade, F., Mabrouki, T., Raïssi, K., 2002, Prédiction du comportement vibratoire du fraisage latéral de finition des pièces à parois minces, Mécanique et Industrie, 3:403-418.
 [10] Thevenot, V., Arnaud, L., Dessein, G., Cazenave-Larroche, G., 2004, Influence of material removal on dynamic behavior of thin walled structure in peripheral milling, Seventh CIRP International workshop on Modelling of Machining Operation, Cluny, France.
 [11] Budak, E., 1994, Mechanics and dynamics of milling thin walled structures, Phd. Thesis, University of British Columbia.
 [12] Thevenot, V., Arnaud, L., Dessein, G., Cazenave-Larroche, G., 2006, Integration of dynamic behaviour in stability lobes method: 3D lobes construction and application to thin walled structure milling, International Journal of Advanced Manufacturing Technology, 27:638-644.
 [13] Bravo, U., Altuzarra, O., López de Lacalle, L.N., Sanchez, J.A., Campa, F.J., 2005, Stability limits of milling considering the flexibility of the workpiece and the machine, International Journal of Machine Tools and Manufacture, 45:1669-1680.
 [14] Smith, S., Dvorak, D., 1998, Tool path strategies for high speed milling aluminium workpieces with thin webs, Mechatronics, 8:291-300.
 [15] Altintas, Y., 2001, Analytical prediction of three dimensional chatter stability in milling, The Japan Society of Mechanical Engineers, International Journal Series, 44:717-723.
 [16] Campa, F.J., López de Lacalle, L.N., Bravo, U., Herranz, S., Ukar, E., 2005, Determination of cutting conditions for the stable milling of flexible parts by means of a three-dimensional dynamic model, Proceedings of International Mechanical Engineering Congress and Exposition, Orlando Florida.